

O. SILVESTRE¹
M.C. PUJOL^{1,✉}
M. RICO²
F. GÜELL¹
M. AGUILÓ¹
F. DÍAZ¹

Thulium doped monoclinic KLu(WO₄)₂ single crystals: growth and spectroscopy

¹ Física i Cristal·lografia de Materials (FiCMA), Universitat Rovira i Virgili, Campus Sescelades, c/ Marcell·l Domingo, s/n, 43007 Tarragona, Spain

² Instituto de Ciencia de Materiales de Madrid, Consejo Superior de Investigaciones Científicas, c/ Sor Juana Inés de la Cruz 3, Cantoblanco, 28049 Madrid, Spain

Received: 22 November 2006/Revised version: 26 March 2007
© Springer-Verlag 2007

ABSTRACT This paper presents the crystal growth and optical characterization of thulium-doped KLu(WO₄)₂ (KLuW). Thulium-doped KLuW macrodefect-free monoclinic single crystals ($a^* \times b \times c \approx 10 \times 7 \times 15 \text{ mm}^3$) were grown by the top seeded solution growth slow cooling method with dopant concentrations of 0.5%, 1%, 3% and 5% atomic in solution. The evolution of unit cell parameters in relation with thulium doping was studied by X-ray powder patterns. Thulium energy levels in the KLuW host were determined by 6 K polarized optical absorption. The Judd–Ofelt parameters determined were $\Omega_2 = 9.01 \times 10^{-20} \text{ cm}^2$, $\Omega_4 = 1.36 \times 10^{-20} \text{ cm}^2$ and $\Omega_6 = 1.43 \times 10^{-20} \text{ cm}^2$. The maximum emission cross section for the 1.9 μm emission, calculated by Füchtbauer–Ladenburg method, is $1.75 \times 10^{-20} \text{ cm}^2$, at 1845 nm with $E//N_m$. The intensity decay time from the emitting levels 1G_4 and 3H_4 levels in relation to the concentration were studied. For the lowest thulium concentration, the measured decay times from 1G_4 and 3H_4 emitting levels are 140 μs and 230 μs , respectively.

PACS 42.55.Rz; 78.20.-e; 78.55.-m

1 Introduction

There is increasing interest in finding new solid state laser systems emitting at around 2 μm . At this wavelength range, there is a line of water absorption in the “eye-safe” region. This causes a large number of applications of this emission such as surgery and other medical laser applications, and remote sensing of the atmosphere (LIDAR devices). Thulium ion can be efficiently lased at this emission range, and the thulium electronic transition $^3H_6 \rightarrow ^3H_4$ can be pumped by diode lasers.

The monoclinic KRE(WO₄)₂; RE = Y, Gd and Lu (hereafter KREW) crystals are a promising material for obtaining a multi-Watt diode laser pumped thulium laser, because in these hosts, the $^3H_6 \rightarrow ^3H_4$ absorption band of thulium is located around 800 nm and is broader than in other solid state laser hosts. These features of thulium spectroscopy in KREW, mean that they can be pumped by AlGaAs, an existing diode laser pump for the Nd³⁺ ion.

The monoclinic KREW compounds are well-known as solid laser hosts [1]. The feasibility of growing highly doped ytterbium KLuW material [2] and the excellent results of its ytterbium laser action [3]; are good enough reasons for growing Tm:KLuW single crystals and studying thulium spectroscopy in KLuW.

Furthermore, Tm laser action has already been successfully achieved in KLuW. CW laser oscillation has been obtained in the 1.9 μm range with both Ti:sapphire and diode laser pumping near 800 nm for both polarizations, $E//N_m$ and $E//N_p$. The maximum output powers were 1.4 and 4 W, respectively, and the corresponding slope efficiencies with respect to the absorbed power were 60% and 69%, respectively. Tuning has also been studied for the two polarizations with Ti:sapphire pumping ranging from 1800 to 1987 nm. In the case of no polarization selective cavity elements, the diode-pumped Tm:KLu(WO₄)₂ laser naturally selected the $E//N_m$ polarization [4]. In these Tm:KGdW and Tm:KYW crystals 1.9 μm laser emission has also been achieved [5], [6–9]. The success of the laser operation justifies a deeper study of the spectroscopy of Tm³⁺ ions in KLuW host.

In the present study, we report the growth of macrodefect-free single crystal Tm:KLuW in the range 0.5–5% atomic Tm doping level in the solution by top seeded solution growth-slow cooling (TSSG-SC). A detailed study of thulium spectroscopy in this host is presented. Polarized optical absorption (OA) and photoluminescence (PL) at low temperature (LT) were used to determine the Stark levels of Tm³⁺ in KLuW. Polarized OA at room temperature (RT) was measured to determine the range of pumping and absorption cross-section. Emission cross section calculations were made using the Füchtbauer–Ladenburg (F–L) method. Experimental polarized emission spectra were performed at RT and LT in 1.9 μm range. Radiative lifetimes were calculated using the Judd–Ofelt (J–O) formalism [10, 11]. Photoluminescence measurements were measured in order to characterize the laser emission channels in this host.

2 Experimental

Tm:KLuW crystals were grown by the TSSG-SC method using K₂W₂O₇ as the solvent and a growth methodology described elsewhere [12, 13]. The chemical composition

✉ Fax: +34-977559563, E-mail: mariacinta.pujol@urv.cat

of the single crystals was measured by electron probe microanalysis (EPMA) using a Cameca Camebax SX 50. For the constitutional elements K, W, Lu and O, the undoped KLuW single crystal was used as the standard reference. The L_{α} line and the REE2 standard (P&H Developments) were used to measure thulium concentration.

X-ray powder diffraction analysis was performed on a Siemens D-5000 diffractometer (Bragg–Brentano para-focusing geometry and vertical θ – θ goniometer) to obtain the unit cell parameters. The X-ray powder diffraction patterns were recorded at $2\theta = 10$ – 70° (size step = 0.02° , and step time = 16 s). The samples were obtained with a $[\text{Tm}^{3+}]$ (% solute in moles) = 3, 5, 7.5, 10 and 20 in solution. The crystals used for structural studies were obtained from high temperature solutions, with $\text{K}_2\text{W}_2\text{O}_7$ as the solvent, and a solution composition of 11.5% mol solute and 88.5% mol solvent. The crystals nucleated on a 12 mm diameter platinum disc rotating at 40 rpm in the homogeneous solution. The crystals grew because of the supersaturation caused by lowering the temperature about 10 K from the saturation temperature, at a cooling rate of about 0.5 K h^{-1} .

Polarized optical absorption was performed at RT and 6 K using a Cary Varian 500 spectrophotometer, with a resolution of 0.025 nm in the UV-VIS region and 0.2 nm in the NIR region. An Oxford Instruments cryostat (SU 12 model) with helium-gas close-cycle flow was used to cool the samples in the low-temperature experiments. The sample was a parallelepipedic prism with the faces parallel to a principal optical plane (N_g – N_m plane, N_g – N_p plane and N_m – N_p plane) so that polarized measurements could be taken. The location of the principal optical axis and optic axes in KLuW is described elsewhere [2].

Room temperature and LT emission spectra were measured at 90° to the pumping direction and were excited at 802 nm and 795 nm (12469 cm^{-1} and 12579 cm^{-1} , respectively). For these emission spectra measurements we used two different set-ups: 1) the samples was excited with a narrow linewidth BMI VEGA 100 optical parametric oscillator pumped by the third harmonic of a Q-switched BMI SAGA 120 Nd:YAG laser (pulse duration: 7 ns, repetition rate: 10 Hz). Photoluminescence was dispersed through a HR460 Jobin Yvon-Spex monochromator (focal length: 460 mm, $f/5.3$, spectral resolution: 0.05 nm). The gratings used had 600 grooves/mm blazed at $1 \mu\text{m}$ and 300 grooves/mm grating blazed at $2 \mu\text{m}$. The detectors applied were Hamamatsu: R928 and R5509-72 NIR photomultipliers. They were connected to a Perkin Elmer 7265DSP lock-in amplifier. 2) For 1.5 and $1.9 \mu\text{m}$ emission experiments, the pumping was a Ti:sapphire laser, Spectra Physics model 3900. The emission was analyzed with a Spex 340E spectrometer ($f = 34 \text{ cm}$) and detected with a Ge photodiode, model ADC-403 IR ($\lambda \approx 1.0$ – $1.7 \mu\text{m}$), and photovoltaic detector Hamamatsu InSb P5968-060 ($\lambda \approx 1.1$ – $5.5 \mu\text{m}$) amplified by a C4159-01 preamplifier, cooled at 77 K for both of them. These were connected to a computer through a lock-in amplifier EG&G Princeton Applied Research, model 52091.

The experimental set-up for decay time measurements was the same as the first described for PL experiments, and time decay curves were recorded using a Tektronix TDS-714 digital oscilloscope.

3 Results and discussion

3.1 Crystal growth

Macrodefect-free thulium doped KLuW single crystals have been grown by the TSSG-SC method. Crystal growth experiments were carried out in the temperature range between 1167 and 1180 K and with a solution made up of a 11.5/88.5 (solute/solvent) molar ratio. To obtain samples with different thulium concentrations, four different $\text{Tm}_2\text{O}_3/(\text{Lu}_2\text{O}_3 + \text{Tm}_2\text{O}_3)$ ratios of thulium oxide substitution were set at 0.005, 0.01, 0.03 and 0.05. The precursor oxides K_2CO_3 (Fluka, 99.0%), Lu_2O_3 (Aldrich, 99.9%), Tm_2O_3 (Aldrich, 99.9%) and WO_3 (Fluka, 99.9%) were melted in the platinum crucible. The crucible was located in a vertical furnace in such a way that the axial temperature gradient in the solution was about 0.13 K mm^{-1} (hot bottom), while the radial temperature gradient was about 0.1 K mm^{-1} (hot crucible wall).

After the solution had been homogenized, the saturation temperature was determined with a KLuW b -oriented seed in contact with the free surface, at the center, of the solution. Then, the growth process began on KLuW seed, while the solution temperature was decreased by about 10–20 K at a rate between 0.2 K h^{-1} for 0.5 and 1% Tm, and 0.1 K h^{-1} for 3 and 5% Tm. The cooling rate was different because macrodefects were present in the 3% and 5% Tm crystals grown at 0.2 K h^{-1} . The crystal rotation was 40 rpm. The crystal growth conditions allowed an average growth rate of 0.025–0.040 g/h. After 4–8 or 8–10 days of growth, depending on the cooling rate, the crystals were slowly removed from the solution and cooled to RT at 15 K h^{-1} to avoid thermal shocks.

In summary, the dimensions of the crystals grown using a b -oriented seed were typically 14.1 – $15.2 \text{ mm} \times 9.3$ – $11.1 \text{ mm} \times 5.4$ – 7.5 mm in the c , a^* and b directions, respectively. The photograph in Fig. 1 shows an example of a grown Tm:KLuW doped crystal. The crystals grown weighted between 2.8 and 5 g. Table 1 summarizes the main details of crystal growth.

The distribution coefficient of the thulium in KLuW was determined by

$$K_{\text{Lu}^{3+}} = \frac{(\text{moles Tm}^{3+}/(\text{moles Tm}^{3+} + \text{moles Lu}^{3+}))_{\text{crystal}}}{(\text{moles Tm}^{3+}/(\text{moles Tm}^{3+} + \text{moles Lu}^{3+}))_{\text{solution}}} \quad (1)$$

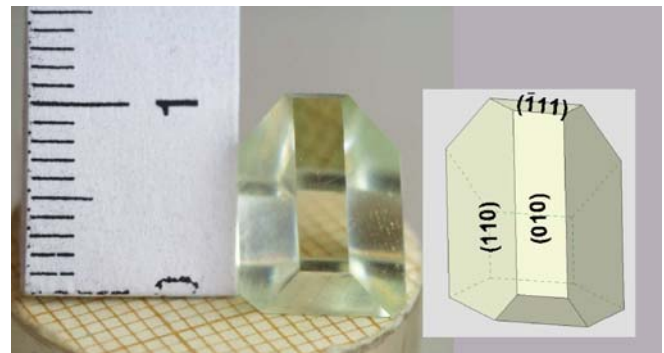


FIGURE 1 Photograph of KLuW doped with thulium single crystal grown in the b direction and morphological scheme

A	B	C	D	E	F	G	H	I	J	K	L
0.13	0.5% Tm	<i>b</i>	0.2	20	3.9716	397	none	14.1	11.1	7.47	1174.6
0.13	1% Tm	<i>b</i>	0.2	20	3.6277	362	none	14.30	10.11	5.4	1168.8
0.13	3% Tm	<i>b</i>	0.1	20	5.6229	281	none	11.32	9.28	7.15	1179.1
0.13	5% Tm	<i>b</i>	0.1	20	4.986	249	none	15.2	10.4	7.5	1178.5

A: Temperature gradient in the solution, K mm⁻¹; B: Tm₂O₃/(Lu₂O₃ + Tm₂O₃) ratio in the solution, atom %; C: seed orientation; D: cooling rate, K h⁻¹; E: cooling interval, K; F: crystal weight, g; G: growth rate (× 10⁻⁴), g h⁻¹; H: macrodefects; I: crystal dimensions along *c* direction, mm; J: crystal dimensions along *a** direction, mm; K: crystal dimensions along *b* direction, mm; L: growth temperature, K

TABLE 1 Details of crystal growth of the KLu_{1-x}Tm_x(WO₄)₂ single crystals

<i>x</i>	<i>K</i>	[Tm ³⁺] (cm ⁻³)	% weight	Stoichiometric formula
0.5%	0.006	1.08	3.51 × 10 ¹⁹	KLu _{0.994} Tm _{0.006} (WO ₄) ₂
1%	0.012	1.17	7.60 × 10 ¹⁹	KLu _{0.988} Tm _{0.012} (WO ₄) ₂
3%	0.037	1.23	2.41 × 10 ²⁰	KLu _{0.963} Tm _{0.037} (WO ₄) ₂
5%	0.050	1.00	3.25 × 10 ²⁰	KLu _{0.950} Tm _{0.050} (WO ₄) ₂

TABLE 2 Summary of the EPMA results of KLu_{1-x}Tm_x(WO₄)₂ single crystals

These measurements provide a distribution coefficient of Tm³⁺ (1.00–1.23), roughly to unity. This indicates that it is possible to obtain homogeneously doped single crystals, which is desirable in order to improve the laser action parameters. Table 2 summarizes the EPMA results; we like to note that the detection limit of Tm ions in KLuW by EPMA technique is 0.016% weight. This value is lower than our concentrations present in this work.

3.2 Unit cell parameters as a function of thulium doping

KLu(WO₄)₂ crystals are monoclinic with *C*₂/*c* space group. The unit cell parameters for undoped KLuW are *a* = 10.576(7) Å, *b* = 10.214(7) Å, *c* = 7.487(2) Å and β = 130.68(4)° [2]. As this material is important as a host for lanthanide doping, the measurement of the change in the unit cell parameters is useful for predicting the structural changes related to the doping and the mismatch for epitaxial film growth [14].

The real composition in the crystal was calculated taking into account the distribution coefficient of thulium in KLuW in our growth experiments, calculated from the quan-

titative analysis by EPMA. As expected, the structure remains isostructural in all cases (the material KTm(WO₄)₂ is also isostructural [15]). In order to obtain the cell parameters, the X-ray powder diffraction patterns were fitted using the FULLPROF program [16] and the crystalline structure of KLuW obtained from single crystal diffraction as a structural model. Figure 2 shows the evolution of the unit cell parameters of KLuW as a function of the thulium doping. The unit cell parameters *a*, *b* and *c* increase and β remains basically constant when the Tm concentration increases. This behavior is expected because of the increase in the ionic radius of Tm (0.994 Å) in relation with Lu (0.977 Å). The ionic radius values are taken from Shannon [17] for a coordination number of 8.

3.3 Thulium absorption in KLuW

Tm³⁺ has an even number of active electrons, 4*f*¹², and is located in *C*₂ symmetry site (substitution of Lu³⁺) as we demonstrated previously in other rare-earth ions. Optical absorption (OA) was been measured with light polarized parallel to the three principal optical axes of the KLuW crystal. As we mentioned above, a parallelepipedic prism-shaped sample whose faces were parallel to a principal optical plane (*N*_g–*N*_m plane, *N*_g–*N*_p plane and *N*_m–*N*_p plane) was used to make polarized measurements.

The splitting of the different manifolds is in agreement with its multiplicity, assuming only one center for Tm³⁺ ion with *C*₂ symmetry. Figure 3 shows the polarized OA measurements in KLu_{0.994}Tm_{0.006}(WO₄)₂ at LT (6 K). When the temperature decrease, extra peaks caused by the thermal population of the various sublevels of the ground state and possible vibronic (electron–phonon interaction) peaks are eliminated. Table 3 shows around 67 energy levels (Stark levels) of Tm³⁺ that were determined in the range studied. To our knowledge, this is the first time that the splitting of Tm³⁺ in KLuW has been determined. The Stark splitting of a given manifold is larger in Tm:KLuW than in Tm:KGdW; so the strength of the crystal field is largest in KLuW host; this also means that the splitting in the ground state manifold is broader, which reduces the thermal population of the upper

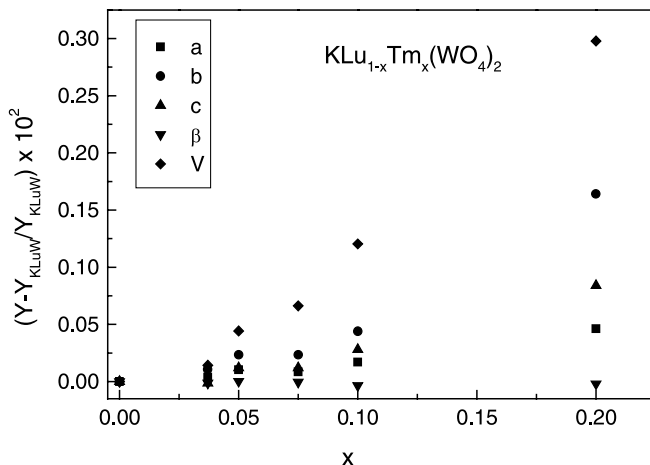


FIGURE 2 Evolution of unit cell parameters of KLu_{1-x}Tm_x(WO₄)₂ with thulium doping

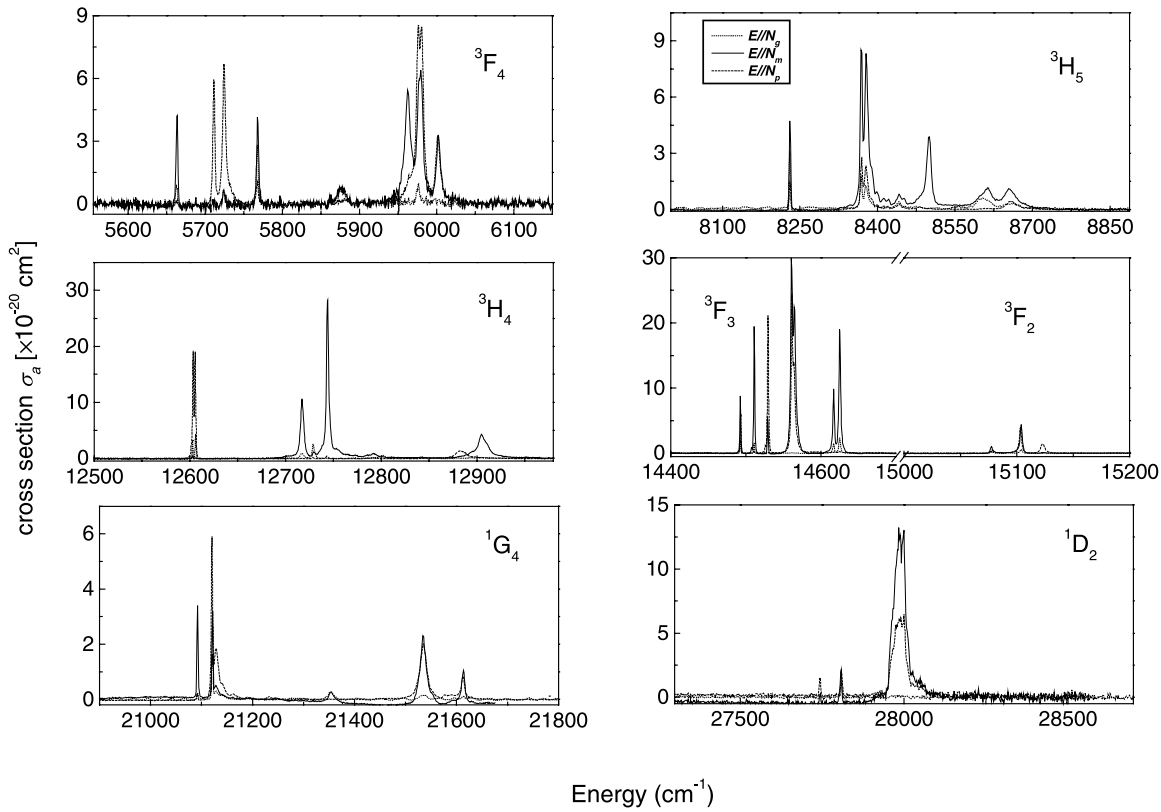


FIGURE 3 Low temperature (6 K) optical absorption of KLuW single crystal doped with thulium, and recorded with light polarized parallel to the three principal optical axes

$2S+1L_J$	$E//N_{g,p,m}$	$E_{\text{exp}} (\text{cm}^{-1})$	$2S+1L_J$	$E//N_{g,p,m}$	$E_{\text{exp}} (\text{cm}^{-1})$	$2S+1L_J$	$E//N_{g,p,m}$	$E_{\text{exp}} (\text{cm}^{-1})$	
3H_6		0	3H_5	p(gm)	8389	3F_2	gm(p)	15078	
		135		p(gm)	8441		gm(p)	15081	
		155		m	8452		gp	15103	
		224		m	8481		p	15123	
		247		m	8500		–	–	
		256		gm	8599				
		279		gm	8612	1G_4	gm(p)	21092	
		329		p(gm)	8654		p(gm)	21121	
		346					p(gm)	21128	
		359		3H_4	p(gm)		12603	m	21233
		513			p(gm)		12606	gm	21353
		522			gm		12717	gm	21361
		530			gm		12729	p(gm)	21535
		m(p)	12744		p		21581		
		m	12790		p(gm)	21613			
		g	12801						
		p	12883		1D_2	p(m)	27743		
		m	12906	p(m)		27808			
3F_4	gm(p)	5663	3F_3	gm(p)		14493	m(p)	27987	
	p(gm)	5711		m(p)		14511	m(p)	28000	
	p(gm)	5724		m(p)		14529	p(m)	28050	
	gm(p)	5768		gm	14561				
	gm(p)	5876		gm	14564				
	m(p)	5963		gm	14617				
	p(gm)	5976		m(p)	14625				
	p(m)	5981							
p(m)	6002								
3H_5	gm(p)	8231							
	p(gm)	8369							
	p(gm)	8379							

TABLE 3 Experimental energy levels, E_{exp} , (in cm^{-1}) and polarization label, $E//N_{g,p,m}$, of Tm^{3+} ions observed in the KLuW single crystal. The energy values of the Stark levels have been obtained experimentally by optical absorption and for the ground state, by photoluminescence at 6 K

sublevels of the ground state in the 2 μm laser quasi-four level laser performance.

The polarization character of every peak was determined by experimental observation. Generally, the spectra recorded

with $E//N_m$ show all the peaks corresponding to the transition between the first excited sublevel of the ground state and the sublevels of the excited state; independently of the selection rule. The peaks were assigned by comparing the intensity

of the N_g and N_p polarizations. The label (not in brackets) in Table 3 indicates the polarization character of every peak; while the one in brackets indicates that the peak is also present in the other polarization. Unfortunately, it cannot be assigned the symmetry to the first sublevel of the ground state. Figure 4 shows the low temperature absorption from the first sublevel of the ground state to manifolds 3H_4 and 3F_4 . In both cases, the J of the terminal state of the absorption is 4, so the expected splitting following the symmetry rule must be $5\Gamma_1 + 4\Gamma_2$, where Γ_1 and Γ_2 are irreducible representations (IR). In the ${}^3H_6 \rightarrow {}^3F_4$ absorption, there are five peaks in the $E//N_p$ absorption spectra and four peaks in $E//N_m$, which suggests that the first sublevel of the ground manifold belongs to the IR Γ_1 . However we must expect the same behavior in relation with symmetry rules the ${}^3H_6 \rightarrow {}^3H_4$ absorption transition in Fig. 4; in this case four peaks are present with $E//N_m$ and $E//N_g$ and five peaks are present with $E//N_p$. Hence the irreducible representation symmetry of the first sublevel of the ground state can not be deduced.

Figure 5a shows the contributions from the thermally populated excited levels (135, 224 and 329 cm^{-1}) of the 3H_6 multiplet at RT. The absorption maximum at RT with $E//N_m$, at 801.8 nm wavelength where it is pumped for the laser experiments [4], belongs to a transition from the second sublevel of the ground state.

In Fig. 6 can be observed the polarized OA in KLu_{0.994}Tm_{0.006}(WO₄)₂ at RT in the 350–1900 nm range. The absorption cross section, σ_a , of the 3H_4 manifold of Tm³⁺ is the highest respect to all the manifolds. For $E//N_p$ polarization, the highest intensity of absorption is at 793.6 nm with a $\sigma_a = 10.5 \times 10^{-20} \text{ cm}^2$ (bandwidth 1.4 nm). Meanwhile, for $E//N_m$ polarization at 801.8 nm the $\sigma_a = 5.6 \times 10^{-20} \text{ cm}^2$ (bandwidth 4 nm). These peaks are suitable for diode-pumping and their σ_a are slightly higher than those of Tm:KGd(WO₄)₂ (KGdW) [18], Tm:KY(WO₄)₂ (KYW) [19] and Tm:KYb(WO₄)₂ (KYbW) [20] and almost twice as the high as that of the disordered tungstate Tm:NaGd(WO₄)₂ (NGdW) [21, 22].

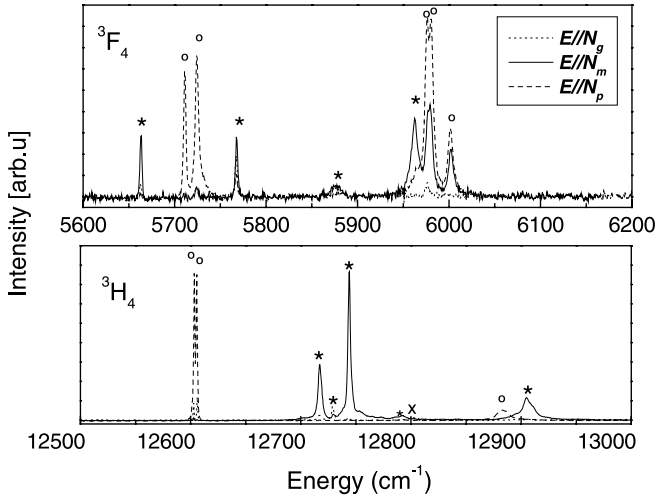


FIGURE 4 Details of the polarized absorption recorded of the Stark levels of the 3H_4 and 3F_4 levels of Tm:KLuW at low temperature. The symbols \star , \circ and \times denote the polarization character for $E//N_m$, $E//N_p$ and $E//N_g$ respectively, attributed to the observed peaks

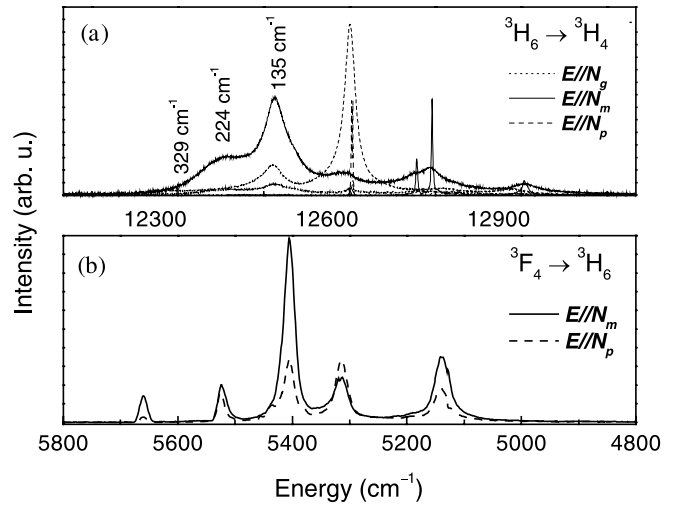


FIGURE 5 (a) Thermal evolution of the polarized optical absorption ${}^3H_6 \rightarrow {}^3H_4$ transition in Tm:KLuW. Spectra at 6 K (continuous line) and the spectra at 300 K (dashed line). The additional bands observed at RT arise from the thermal population of the first excited 3H_6 Stark sublevels. (b) 2 μm PL of Tm:KLuW single crystal at 6 K

We calculated the J–O parameters of Tm³⁺ in KLuW taking into account the biaxial character of the crystal and we shall compare this with those also performed for Tm³⁺ in other crystals. The optical absorptions from the ground state 3H_6 to the 7 excited manifolds: 1D_2 , 1G_4 , ${}^3F_3 + {}^3F_2$, 3H_4 , 3H_5 and 3F_4 were taken into account. In order to apply the J–O theory, the 300 K polarized optical absorption spectra of Tm³⁺ in KLu(WO₄)₂ ($[Tm]_{\text{crystal}} = 0.35 \times 10^{19} \text{ cm}^{-3}$) have been used. Table 4 shows the integrated absorption cross sections, $\Gamma_{JJ'}/[Tm]$, for $E//N_g$, $E//N_m$ and $E//N_p$ spectra. These experimental results have been averaged as $(E//N_g + E//N_m + E//N_p)/3$ and used to achieve the experimental oscillator strengths, f_{exp} , for each excited multiplet as

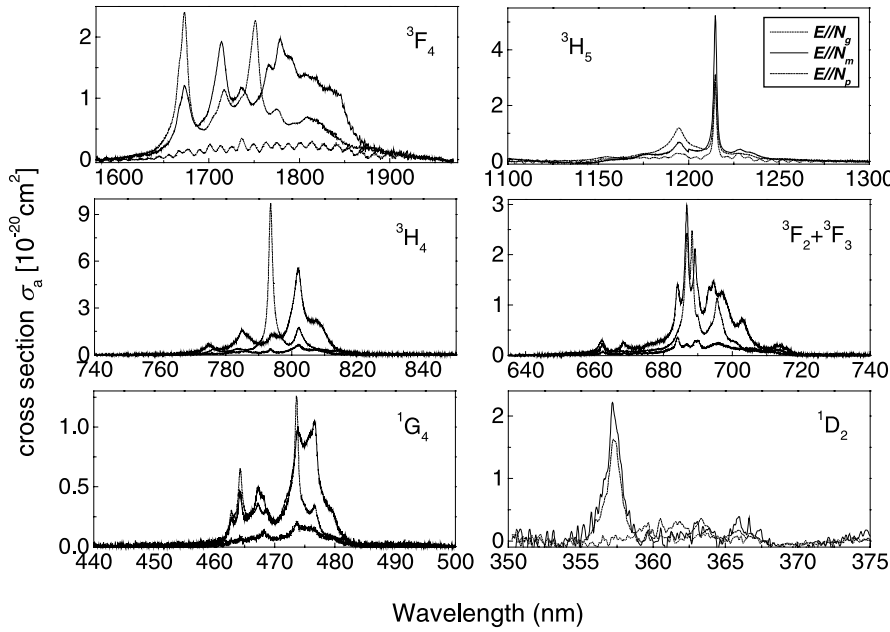
$$f_{\text{exp}} = \frac{4\epsilon_0 m c^2}{e^2 \lambda^2} \frac{\Gamma_{JJ'}}{[Tm]}. \quad (2)$$

The experimental average oscillator strengths obtained by us for Tm³⁺ in KLuW are larger than those reported in a previous work for KGdW, KYW hosts. The J–O theory has been described in a large number of works and details of the treatment can be found elsewhere [23]. We shall just mention that the ED oscillator strengths, $f_{\text{ED,exp}}$, can be obtained as

$$f_{\text{ED,cal}} = \chi \frac{8\pi^2 m c}{3\hbar \lambda (2J+1)} S_{JJ'}, \quad (3)$$

$$S_{JJ'} = \sum_{k=2,4,6} \Omega_k |\langle f^n[L, S]J \| U^k \| 4f^n[L', S']J' \rangle|^2, \quad (4)$$

where Ω_k are the J–O parameters to be obtained from the minimization of the $f_{\text{exp}} - f_{\text{cal}}$ differences. Table 5 includes the Ω_k sets obtained for Tm³⁺ in the KLuW considered here and other materials doped with Tm. In this calculation we have used the $(\|U^k\|)$ matrix elements provided previously by Weber et al. [24], refractive index using the Sellmeier values of KLuW [2] and the accuracy of the J–O parameters is given by the goodness of the least-squares fitting used, root mean square value (rms); also indicated in Table 4. Magnetic dipolar (MD) contributions to the experimental oscillator strengths


FIGURE 6 RT polarized absorption cross-sections of Tm^{3+} in KLuW single crystal

${}^3\text{H}_6 \rightarrow$	$E//N_g$			$E//N_m$		$E//N_p$		$\Gamma/[\text{Tm}]$ (10^{-27} cm^3)	$\bar{f}_{\text{ED,exp}}$ ($\times 10^8$)	$f_{\text{ED,cal}}$ ($\times 10^8$)
	$\bar{\lambda}$ (nm)	$\Gamma_g/[\text{Tm}]$ (10^{-27} cm^3)	$f_{\text{ED,exp}}$ ($\times 10^8$)	$\Gamma_m/[\text{Tm}]$ (10^{-27} cm^3)	$f_{\text{ED,exp}}$ ($\times 10^8$)	$\Gamma_p/[\text{Tm}]$ (10^{-27} cm^3)	$f_{\text{ED,exp}}$ ($\times 10^8$)			
${}^1\text{D}_2$	360	0.56	49.8	3.66	324	3.20	284	2.47	216	294
${}^1\text{G}_4$	472	2.02	101	8.80	447	5.87	300	5.57	282	208
${}^3\text{F}_2 + {}^3\text{F}_3$	688	6.50	156	32.34	767	19.20	458	19.34	462	510
${}^3\text{H}_4$	795	9.40	170	61.42	1090	39.60	708	36.81	658	710
${}^3\text{H}_5$	1214	19.32	148	89.97	690	43.76	336	51.02	391 ^a	309
${}^3\text{F}_4$	1767	43.87	156	249.54	903	186.32	691	159.91	579	581

^a Magnetic dipole (MD) contributions, f_{MD} , were evaluated and discounted as follows ($E//N_g$ 0.69×10^{-6} , $E//N_m$ 0.67×10^{-6} , and $E//N_p$ 0.65×10^{-6})

TABLE 4 Average wavelength, $\bar{\lambda}$, integrated OA cross section, $\Gamma/[\text{Tm}]$, experimental ED oscillator strength, $f_{\text{ED,exp}}$, averaged ED oscillator strength, $\bar{f}_{\text{ED,exp}}$, and calculated ED oscillator strength, $f_{\text{ED,cal}}$, for ${}^{2S+1}L_J$ multiplets of the Tm^{3+} ion in KLuW using J–O parameters Ω_k ($10 \times 10^{-20} \text{ cm}^2$): $\Omega_2 = 9.01$, $\Omega_4 = 1.36$ and $\Omega_6 = 1.43$ and the fit quality obtained with the Ω_k J–O parameter set is described by $\text{rms}(\Delta f)$ ($\times 10^{-6}$) = 0.88

Host	Ω_2 ($\times 10^{20} \text{ cm}^2$)	Ω_4 ($\times 10^{20} \text{ cm}^2$)	Ω_6 ($\times 10^{20} \text{ cm}^2$)	Ref.
KLuW	9.01	1.36	1.43	This paper
KYW	10.673	2.481	1.344	[9]
KGdW	2.64	5.84	14	[38]
NGdW	9.48	1.28	1.36	[21]
NGdW	5.012	1.355	4.594	[22]
YAP	0.67	2.30	0.74	[39]
YAG	0.7	1.2	0.5	[40]
LiYF ₄	2.43	1.08	0.67	[41]
BaYb ₂ F ₈	1.2	0.94	1.2	[42]
YVO ₄	9	1.05	2.27	[43]

TABLE 5 The Judd–Ofelt parameter (Ω_k) set of Tm^{3+} in KLuW and in other relevant solid-state laser hosts

were also taken into account to calculate the electrical dipole (ED) contribution, $f_{\text{ED,exp}}$. Expressions for these contributions can be found elsewhere [23].

Using the calculated Ω_k sets, the radiative rates, $A_{JJ'}$ were obtained as described in the literature [23] and from them the branching ratios, $\beta_{JJ'} = A_{JJ'} / \sum_{J'} A_{JJ'}$, and the radiative lifetimes, $\tau_{\text{rad}} = 1 / \sum_{J'} A_{JJ'}$ of the luminescence were calculated. Table 5 shows a comparison of the Judd–Ofelt parameters of Tm^{3+} among several laser solid state hosts and our laser crystal. The Ω_k set corresponding to Tm^{3+} in KLuW presents a similar behavior and values in the double

tungstates and molybdates than other matrices compared. Finally, we summarize in Table 6 the results obtained for Tm^{3+} in $\text{KLu}(\text{WO}_4)_2$ single crystal from J–O calculations.

3.4 Emissions spectra study

Figure 7 shows the energy level diagram of Tm^{3+} ions and observed emissions in KLuW host. We can see the different excitations used and emissions observed experimentally. Figure 8 shows the room temperature emission channels of $\text{KLu}_{0.963}\text{Tm}_{0.037}(\text{WO}_4)_2$, under infrared pumping at

Transition	λ (nm)	$A_{ED} + A_{MD}$ (s ⁻¹)	β_{ij} %	τ_{rad} (μ s)
$^1D_2 \rightarrow ^1G_4$	1493	743	1	13
3F_2	777	2730	4	
3F_3	749	4719	6	
3H_4	658	24039	32	
3H_5	510	290	0	
3F_4	452	22784	30	
3H_6	363	19597	26	86
$^1G_4 \rightarrow ^3F_2$	1623	35	0	
3F_3	1505	130	1	
3H_4	1176	69	1	
3H_5	775	2222	19	
3F_4	648	5290	45	
3H_6	480	3903	34	200
$^3F_2 \rightarrow ^3F_3$	20746	0+0.02	0	
3H_4	4277	54	1	
3H_5	1484	476	10	
3F_4	1078	2944	59	
3H_6	681	1523	30	
$^3F_3 \rightarrow ^3H_4$	5388	2	0	147
3H_5	1598	1361	20	
3F_4	1137	968+153	15	
3H_6	705	4327	65	
$^3H_4 \rightarrow ^3H_5$	2273	139+23	3	203
3F_4	1441	387	8	
3H_6	811	4376	89	
$^3H_5 \rightarrow ^3F_4$	3937	8	1	1331
3H_6	1260	629+114	99	
$^3F_4 \rightarrow ^3H_6$	1853	674	100	1483

TABLE 6 ED and MD transition probabilities, A_{ED} and A_{MD} , branching ratios, β_{ij} , radiative lifetimes, τ_{rad} , of Tm³⁺ in KLuW calculated from the $\Omega_2 = 9.01$, $\Omega_4 = 1.36$, $\Omega_6 = 1.43$ set

802 nm. Six emission channels are present including the emission at 1.9 μ m, in the infrared range: $^3H_4 \rightarrow ^3F_4$ ($E \cong 7143 - 6667$ cm⁻¹, $\lambda \cong 1.41-1.5$ μ m) and $^3F_4 \rightarrow ^3H_6$ ($E \cong 6060-5000$ cm⁻¹, $\lambda \cong 1.65-2$ μ m). In the visible range, the up-conversion emission channels also appears: the $^1D_2 \rightarrow ^3F_4$ transition ($E \cong 22\,222-21\,622$ cm⁻¹, $\lambda \cong 450-462.5$ nm) and the $^1G_4 \rightarrow ^3H_6$ transition ($E \cong 21\,277-20\,408$ cm⁻¹, $\lambda = 470$

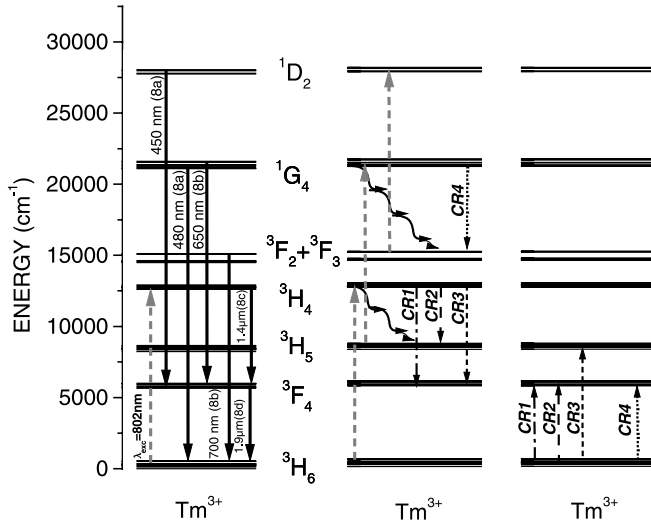


FIGURE 7 Energy diagram of the Stark sublevels of Tm³⁺ ions in KLuW single crystal observed at RT. Arrows indicate radiative and non-radiative processes

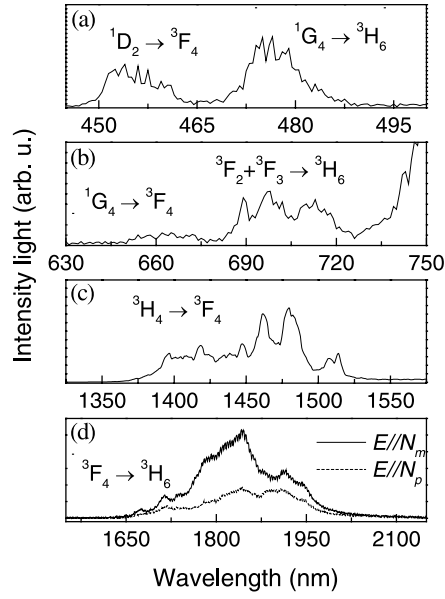


FIGURE 8 RT photoluminescence of Tm:KLuW crystals excited at $\lambda_{exc} \cong 802$ nm. (a) Blue emissions from $^1D_2 \rightarrow ^3F_4$ and $^1G_4 \rightarrow ^3H_6$ transitions. (b) Red emissions from $^1G_4 \rightarrow ^3F_4$ and $^3F_2 + ^3F_3 \rightarrow ^3H_6$ transitions. (c,d) Infrared laser channels of Tm³⁺ corresponding to $^3H_4 \rightarrow ^3F_4$ (1.4 μ m) and $^3F_4 \rightarrow ^3H_6$ (1.9 μ m)

– 490 nm), $^1G_4 \rightarrow ^3F_4$ transition ($E \cong 15\,400-15\,151$ cm⁻¹, $\lambda = 640-660$ nm), and, $^3F_3 + ^3F_2 \rightarrow ^3H_6$ transition ($E \cong 14\,493-13\,889$ cm⁻¹, $\lambda = 690-720$ nm). Unfortunately, we were not recording the ultraviolet emissions of Tm ions because the transparency range is limited to the edge of absorption of KLuW ($\lambda = 365$ nm) [25].

Figure 8d shows the RT polarized photoluminescence at 1.9 μ m when pumping at $12\,466$ cm⁻¹ (802.1 nm) with $E//N_p$ or $12\,472$ cm⁻¹ (801.8 nm) with $E//N_m$, at maximum absorption at 300 K. The emitting level 3F_4 population can be obtained by non radiative relaxation; and also by four cross relaxation processes (CR): CR1 ($^3H_4, ^3H_6 \rightarrow ^3F_4, ^3F_4$); CR2 ($^3H_4, ^3H_6 \rightarrow ^3H_5, ^3F_4$) and CR3 ($^3H_4, ^3H_6 \rightarrow ^3F_4, ^3H_5$) and CR4 ($^1G_4, ^3H_6 \rightarrow ^3F_2 + ^3F_3, ^3F_4$) [26], within the thulium energy levels. It is well-known that the CR1, CR2 and CR3 provide a quantum efficiency value of 2 in this population mechanism. The maximum power of the laser pumping by Ti:sapphire is at $\lambda_L = 1948$ nm with $E//N_m$, which corresponds to the third peak in the experimental spectra for $E//N_m$. The broad spectra lead to a wide range of laser tuning; as reported [4]. The tuning curves were 110 nm ($E//N_m$) and 128 nm ($E//N_p$). The tuning range was similar in Tm:Yb:KYW [27]. For other well-known hosts such as YLF, a tuning range of 162 nm is possible in the cw mode [28] and NGdW with 212 nm tuning range [21].

Low temperature (6 K) emission spectra were also recorded in this range (see also Fig. 5b). It is worth mentioning that at low temperatures the pumping was at 801.9 nm for $E//N_m$ and 793.5 nm for $E//N_p$. The energy sublevels of the ground state are also shown in Table 3. At 300 K, the thermal population in the upper Stark sublevel of the ground state will be 1.94%. The emission was recorded in a polarized way. As can be seen in the figure, the emission was the same in both polarizations; the resolution of the experiment was not enough to

separate the different polarization contributions and identify the polarization character of the emission peaks.

The emission cross sections, σ_e , determined using the reciprocity method (RM) of the thulium-doped KLuW are $\sigma_e = 3.71 \times 10^{-20} \text{ cm}^2$ at 1841 nm for $E//N_m$ and $\sigma_e = 1.58 \times 10^{-20} \text{ cm}^2$ at 1820 nm for $E//N_p$ [4]. The Füchtbauer–Ladenburg (F–L) equation [29] also makes it possible to calculate of the σ_e using the form

$$\sigma_e(\lambda) = \frac{\lambda^5}{8\pi n^2 c \tau_{\text{rad}} f_j \left(\int \lambda I(\lambda) d\lambda \right)} I(\lambda), \quad (5)$$

where n is the refractive index, τ is the measured fluorescence lifetime, f_j is the fraction of the pumped population in the excited state j given by Boltzmann distribution and I is the measured spectral fluorescent intensity. Using the experimental emission spectra of transition ${}^3F_4 \rightarrow {}^3H_6$, the refractive index calculated for each wavelength by Sellmeier equation [2], and the radiative lifetime in bulk sample from J–O and for this radiative transition f_j is equal to 1, we obtained Fig. 9; which compares the σ_e calculated by F–L with the σ_e calculated by RM. The N_g polarization was not taken into account because its absorption was weak, so we assumed that its contribution to this emission could be omitted. From Fig. 9, we can deduce that the effect of reabsorption on the experimental emission at 1.9 μm is still very important, and more so in the N_m emission. The emission cross section calculated by RM does not take this effect into account, but F–L, as it is based on the experimental emission, does. Furthermore, the effect is more pronounced in the $E//N_m$ polarization up to about 1850 nm and less important in the N_p polarization. The radiative lifetime calculated by J–O can also be corroborated

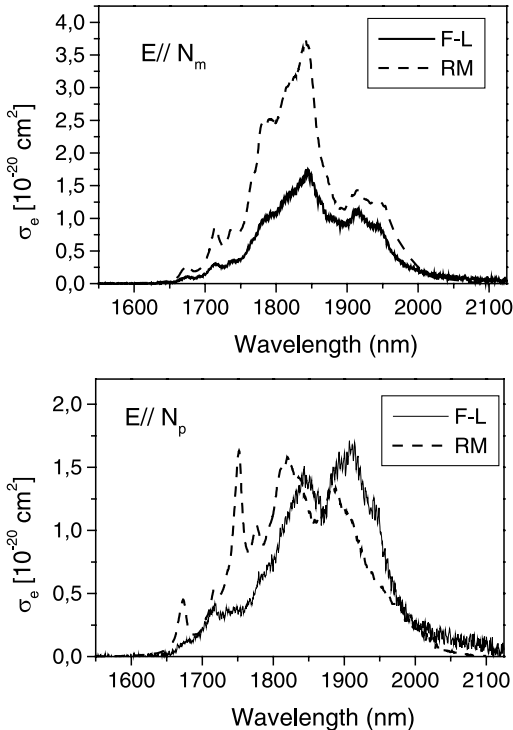


FIGURE 9 Polarized emission cross-section, σ_e , of Tm:KLuW at 300 K by the F–L and reciprocity method

by matching the calculated and measured emission cross sections and solving for τ_{rad} in the Füchtbauer–Ladenburg equation [30, 31]. In this way an average calculated radiative lifetime of around 1.05 ms is obtained. This value agrees rather well with the experimental radiative lifetime measured by the pinhole method [4] and we obtain a quantum efficiency of luminescence to $\eta = 61\%$. The pinhole method measurement of lifetime eliminates the reabsorption contributions to the decay time.

3.5 Decay time measurements

The fluorescence dynamics of the 1G_4 and 3H_4 emitting levels was investigated as a function of the Tm^{3+} concentration ranging from 0.5 at. % to 5 at. % at room temperature with excitation into the 3H_4 level, $\lambda_{\text{exc}} = 802 \text{ nm}$.

It was observed the experimental decay from the emitting 1G_4 energy level in the radiative transition the ${}^1G_4 \rightarrow {}^3H_6$ transition at 476 nm. The emission of the 1G_4 after the excitation into 3H_4 , could be due to two different processes: nonradiative energy transfer process between two thulium ions connecting these two levels and a two step absorption by a single thulium ion, through a quasi-resonant excited state absorption from 3H_4 level to the 1G_4 level. The 1G_4 nonradiative energy transfer population mechanism has been reported for some other crystals [32]. We have observed no rise time and in relation with thulium concentration, in all the cases the decay is single exponential. As the 3H_4 lifetime is longer than the 1G_4 lifetime, the observed decay time is related with 3H_4 manifold. The decay time is 140 μs at the lowest thulium concentration and decreases to 10 μs at the highest. The values of the decays reported in Table 7, which are about half the lifetime of the 3H_4 state suggest that the 1G_4 level is populated by an energy transfer up-conversion (ETU) process involving two Tm^{3+} ions in the 3H_4 level (${}^3H_4, {}^3H_4 \rightarrow ({}^1G_4, {}^3H_6)$).

The experimental decay curves for the 3H_4 energy level was studied measuring the ${}^3H_4 \rightarrow {}^3H_6$ and ${}^3H_4 \rightarrow {}^3F_4$ transitions at 802 nm with $\lambda_{\text{exc}} = 688 \text{ nm}$ (shown in Fig. 10) and 1.48 μm with $\lambda_{\text{exc}} = 802 \text{ nm}$ (summarized in Table 7). The non exponential character of the decays corresponding to high concentration can be described by the model developed by Inokuti and Hirayama [33]. This model assumes nonradiative energy transfer from an excited Tm^{3+} donor to the surrounding Tm^{3+} ions in the ground state continuously distributed. The time dependence of the light intensity decay follows the law

$$I(t) = I(0) \exp \left[\frac{-t}{\tau_0} - \Gamma \left(1 - \frac{3}{s} \right) \frac{N}{c_0} \left(\frac{t}{\tau_0} \right)^{3/s} \right], \quad (6)$$

where τ_0 is the intrinsic lifetime of the donor in the absence of acceptors, $c_0 = 3/4\pi R_C^3$ is a critical concentration related to the distance R_C at which the donor-trap energy transfer rate equals the spontaneous decay rate and $\Gamma(x)$ is the gamma function evaluated in x . The parameter $s = 6, 8$ or 10 correspond for transfer mechanism of electric dipole–dipole, dipole–quadrupole or quadrupole–quadrupole character respectively.

The decay pattern for the lower concentration can be described as a single exponential, so the value obtained for 0.5%

[Tm ³⁺]	$\lambda_e = 476 \text{ nm}$	$\lambda_e = 1.48 \mu\text{m}$		η
	Decay time (μs)	$\tau \text{ } ^3H_4$ (μs)	W_E ($10^{-3} \mu\text{s}$)	
0.5%	140	230	–	1.13
1%	130	160	1.32	0.79
3%	30	70	9.36	0.35
5%	10	20	45.07	0.10

TABLE 7 Decay times from the emitting 1G_4 and 3H_4 levels of Tm³⁺ in KLuW single crystals at different concentrations [Tm³⁺] with $\lambda_{\text{exc}} = 802 \text{ nm}$

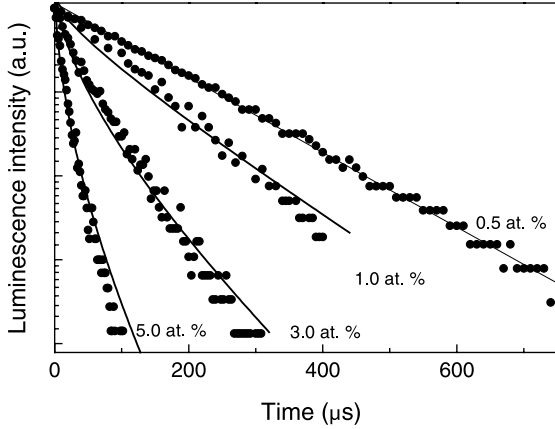


FIGURE 10 Light intensity decays of the 3H_4 photoluminescence of Tm³⁺ in $\text{KLu}(\text{WO}_4)_2$ for different thulium concentrations. $\lambda_{\text{exc}} = 688 \text{ nm}$, $\lambda_e = 802 \text{ nm}$. Results obtained for relatively lower doping concentration of Tm³⁺ in $\text{KLu}(\text{WO}_4)_2$ (0.5%, 1%, 3% and 5%). The lowest concentrations have been fitted a single exponential which provides a lifetime value of 230 μs . However, the fits for 1%, 3%, and 5% Tm doping were obtained using the Inokuti–Hirayama model with $s = 6$. (points are experimental results and solid lines show the fits)

Tm doped sample is $\tau_0 = 230 \mu\text{s}$. The character of the transfer mechanism can be deduced by plotting $\ln[I(t)/I(0)] + t/\tau_0$ versus $t^{3/s}$ and using the τ_0 value obtained for 0.5% Tm doped sample. The decays of 1%–5% Tm-doped samples fit linearly when $s = 6$. Therefore, an electric dipole–dipole non radiative energy transfer is taken place. Figure 10 also shows the fit of the RT experimental decays of level 3H_4 using (6) with $s = 6$ and the corresponding thulium concentration. A good fit is obtained for 3% and 5% Tm doped but shows some deviation at the decay tail. This deviation is likely due to a minor contribution of electric dipole–quadrupole. The fits provides the critical distance, R_C , for each concentration.

Table 8 summarizes the distances obtained. These critical distances can be compared with the average Tm–Tm distances $\bar{r} = (4\pi N/3)^{-1/3}$ for each sample. It is clear that the average Tm–Tm distance in the lowest doped samples is too large in comparison to the critical distance where the cross relaxation phenomena take place, namely $\approx 1.3 \text{ nm}$, therefore energy transfer does not occur and the decays can be expected to be a single exponential as it is indeed found. The average Tm–Tm distance decreases with increasing Tm concentration and it falls into the range where cross relaxation phenomena become activated, therefore the 3H_4 decays become non exponential.

Therefore, at higher thulium concentrations the quenching phenomenon takes place because the Tm–Tm distances decrease and this favors the cross-relaxation mechan-

[Tm ³⁺]	$N \times 10^{20} \text{ (cm}^{-3}\text{)}$	$\bar{r} \text{ (nm)}$	$R_C \text{ (nm)}$
0.5%	0.351	1.90	–
1%	0.760	1.47	1.05
3%	2.41	0.99	1.2
5%	3.25	0.90	1.3

TABLE 8 Average Tm–Tm distance, \bar{r} , for increasing Tm concentration, [Tm³⁺], and critical distance of the cross relaxation phenomena, R_C

isms [34–36]. Table 7 summarizes the decay time studied, the luminescence quantum efficiency η ($\eta = \tau/\tau_{\text{rad}}$) and the cross relaxation rates W_E , by $W_E = 1/\tau - 1/\tau_{\text{rad}}$ (assuming multiphonon decay did not act as a depopulation mechanism) [37]. As mentioned above, the luminescence quantum efficiency decreases as a function of thulium concentration, and consequently W_E increases. Finally, we can deduce that the most relevant losses to reach laser action in 1.5 μm and 1.9 μm would be the transfer energy between Tm ions (see Fig. 10) and cross relaxation processes, which start to appear at thulium concentration higher or equal to 1%, and the blue up-conversion processes pumped at 802 nm where the spectral region overlap AlGaAs diode laser emission. In spite of these losses, 1.9 μm laser emission of Tm ions has been demonstrated with a relatively high optical to optical efficiency [4].

4 Conclusion

In conclusion, we have grown macrodefect-free thulium doped $\text{KLu}(\text{WO}_4)_2$ single crystals up to 5 atomic %, where thulium ions substitute lutetium ions. The distribution coefficient of thulium, around 1, in the growth conditions described assures an high homogeneity of active ions inside the crystal. The increase of thulium doping gives an increase in the unit cell parameters.

A total of 67 energy stark levels of thulium were determined by low temperature (6 K) polarized absorption and emission measurements. The RT absorption measurements were made, and lead at $E//N_p$ polarization, to an absorption cross section value of $10.5 \times 10^{-20} \text{ cm}^2$ (bandwidth 1.4 nm) at 793.5 nm. While for $E//N_m$ polarization at 801.8 nm the absorption cross section is $5.6 \times 10^{-20} \text{ cm}^2$ (bandwidth 4 nm). Emission spectra experiments showed that these materials also have interesting laser channels in the blue and 1.5 μm ranges. More detailed fluorescence spectra were performed in the 1.9 μm range. A broad-band at RT gives the tunability of the material. The radiative lifetimes of the 1G_4 , 3H_4 and 3F_4 states were determined by J–O formalism. Finally the intensity decay time from the emitting 1G_4 and 3H_4 levels in relation with the concentration were determined, and the Tm–Tm interaction was observed to increase as the concentration increased.

ACKNOWLEDGEMENTS We gratefully acknowledge financial support from the Education and Science Ministry of Spain under Project MAT-2004-20471-E, MAT 2005-06354-C03-02 and CIT-020400-2005-14 and from the Generalitat de Catalunya under project 2005SGR658. This paper was also funded by the EU-Commission Project DT-CRYS (STRP-NMP3-CT-2003-505580). M.C. Pujol and M. Rico are supported by the Education and Science Ministry of Spain under the Ramón y Cajal programme.

REFERENCES

- 1 A.A. Kaminskii, Phys. Stat. Solidi A **200**, 215 (2003)
- 2 M.C. Pujol, X. Mateos, A. Aznar, X. Solans, S. Suriñach, J. Massons, F. Díaz, M. Aguiló, J. Appl. Crystallogr. **39**, 230 (2006)
- 3 X. Mateos, V. Petrov, M. Aguiló, R.M. Solé, J. Gavalda, J. Massons, F. Díaz, U. Griebner, IEEE J. Quantum Electron. **QE-40**, 1056 (2004)
- 4 X. Mateos, V. Petrov, J. Liu, M.C. Pujol, U. Griebner, M. Aguiló, F. Díaz, M. Galan, G. Viera, IEEE J. Quantum Electron. **QE-42**, 1008 (2006)
- 5 V. Petrov, F. Güell, J. Massons, J. Gavalda, R.M. Sole, M. Aguiló, F. Díaz, U. Griebner, IEEE J. Quantum Electron. **QE-40**, 1244 (2004)
- 6 A.A. Kaminskii, A.A. Pavlyuk, P.V. Klevtsov, I.F. Balashov, V.A. Berenberg, S.E. Sarkisov, V.A. Fedorov, M.V. Petrov, V.V. Lyubchenko, Inorg. Mater. **13**, 482 (1977) [Translated from Izv. Akad. Nauk. USSR., Neorg. Mater. **13**, 582 (1977)]
- 7 S.N. Bagaev, S.M. Vatik, A.P. Majorov, A.A. Pavlyuk, Adv. Solid State Lasers **50**, 175 (2001)
- 8 A.A. Demidovich, A.A. Kuzmin, N.K. Nikeenko, M. Mond, S. Kück, J. Alloys Compounds **341**, 124 (2002)
- 9 A.E. Troshin, V.E. Kisel, V.G. Shcherbitsky, N.V. Kuleshov, A.A. Pavlyuk, E.B. Dumina, A.A. Kornienko, Adv. Solid State Photon. **98**, 214 (2005)
- 10 B.R. Judd, Phys. Rev. **127**, 750 (1962)
- 11 G.S. Ofelt, J. Chem. Phys. **37**, 511 (1962)
- 12 M.C. Pujol, R. Solé, V. Nikolov, J. Gavalda, J. Massons, C. Zaldo, M. Aguiló, F. Díaz, J. Mater. Res. **14**, 3739 (1999)
- 13 M.C. Pujol, X. Mateos, R. Solé, J. Massons, J. Gavalda, X. Solans, F. Díaz, M. Aguiló, J. Appl. Crystallogr. **34**, 1 (2001)
- 14 A. Aznar, O. Silvestre, M.C. Pujol, R. Solé, M. Aguiló, F. Díaz, Cryst. Growth Des. **6**, 1781 (2006)
- 15 P.V. Klevtsov, L.P. Kozeeva, L.Y. Kharchenko, Sov. Phys. Crystallogr. **20**, 732 (1976) [Translated from Kristallografiya **20**, 1210 (1975)]
- 16 J. Rodríguez-Carvajal, Reference Guide for the Computer Program Fullprof (Laboratoire León Brillouin, CEA-CNRS, Saclay, France, 2000)
- 17 R.D. Shannon, Acta Cryst. A **32**, 751 (1976)
- 18 F. Güell, J. Gavalda, R. Solé, M. Aguiló, F. Díaz, M. Galán, J. Massons, J. Appl. Phys. **95**, 919 (2004)
- 19 S.N. Bagaev, S.M. Vatik, A.P. Majorov, A.A. Pavlyuk, D.V. Plakushchev, Quantum Electron. **30**, 310 (2000)
- 20 M.C. Pujol, F. Güell, X. Mateos, J. Gavalda, R. Solé, J. Massons, M. Aguiló, F. Díaz, G. Boulon, A. Brenier, Phys. Rev. B **66**, 144304 (2002)
- 21 J.M. Cano-Torres, M.D. Serrano, C. Zaldo, M. Rico, X. Mateos, J. Liu, U. Griebner, V. Petrov, F.J. Valle, M. Galán, G. Viera, J. Opt. Soc. Am. B **23**, 2494 (2006)
- 22 H. Wang, G. Jia, F. Yang, Y. Wei, Z. You, Y. Wang, J. Li, Z. Zhu, X. Lu, C. Tu, Appl. Phys. B **83**, 579 (2006)
- 23 C. Görller-Walrand, K. Binnemans, in *Handbook on the Physics and Chemistry of Rare Earths*, ed. by K.A. Gschneider Jr., L. Eyring (Elsevier, Amsterdam, 1998), vol. 25, p. 101
- 24 A.A. Kaminskii, *Crystalline Lasers, Physical Processes and Operating Schemes* (CRC, Boca Raton, New York, London, Tokyo, 1996)
- 25 X. Mateos, R. Solé, J. Gavalda, M. Aguiló, J. Massons, F. Díaz, V. Petrov, U. Griebner, Opt. Mater. **28**, 519 (2006)
- 26 N.A. Barnes, E.D. Filer, C.A. Morrison, C.J. Lee, IEEE J. Quantum Electron. **QE-32**, 92 (1996)
- 27 L.E. Batay, A.A. Demidovich, A.N. Kuzmin, A.N. Titov, M. Mond, S. Kück, Appl. Phys. B **75**, 457 (2002)
- 28 A. Dergachev, K. Wall, P.F. Moulton, Adv. Solid State Lasers **68**, 343 (2002)
- 29 B.F. Aull, H.P. Jossen, IEEE J. Quantum Electron. **QE-18**, 925 (1982)
- 30 L. DeLoach, S.A. Payne, L.L. Chase, L.K. Smith, W.L. Kway, W.F. Krupke, IEEE J. Quantum Electron. **QE-29**, 1179 (1993)
- 31 F.D. Patel, E.C. Honea, J. Speth, S.A. Payne, R. Hutcheson, R. Equall, IEEE J. Quantum Electron. **QE-37**, 135 (2001)
- 32 R. Lisiecki, W. Ryba-Romanowski, T. Lukasiewicz, Appl. Phys. B **81**, 43 (2005)
- 33 M. Inokuti, F. Hirayama, J. Chem. Phys. **43**, 1978 (1965)
- 34 W. Ryba-Romanowski, S. Golab, I. Sokolska, G. Dominiak Dzik, J. Zawadzka, M. Berkowski, J. Fink Finowicki, M. Baba, Appl. Phys. B **68**, 199 (1999)
- 35 F. Güell, X. Mateos, R. Solé, J. Gavalda, M. Aguiló, F. Díaz, J. Massons, J. Luminesc. **106**, 109 (2004)
- 36 M.F. Joubert, S. Guy, S. Cuerq, P.A. Tanner, J. Luminesc. **75**, 287 (1997)
- 37 A. Sennaroglu, A. Kurt, G.J. Özen, J. Phys.: Condens. Matter **16**, 2471 (2004)
- 38 C. Tu, J. Li, Z. Zhu, Z. Chen, Y. Wang, B. Wu, Opt. Commun. **227**, 383 (2003)
- 39 M.J. Weber, T.E. Varitimos, B.H. Matsinger, Phys. Rev. B **8**, 47 (1973)
- 40 W.F. Krupke, IEEE Region VI Conf., Albuquerque, NM (1974), pp. 17–31 (unpublished)
- 41 M. Dulick, G.E. Faulkner, N.J. Cockroft, D.C. Nguyen, J. Luminesc. **48–49**, 517 (1991)
- 42 B.M. Antipenko, Opt. Spektrosk. **56**, 72 (1984)
- 43 F.S. Ermeneux, C. Goutadier, R. Moncorgé, Opt. Mater. **8**, 83 (1997)